Science of Sintering, **44** (2012) 197-210

DOI:10.2298/SOS1202197S

UDK 621.927:669.018

Effect of Milling and Annealing on Microstructural, Electrical and Magnetic Properties of Electrodeposited Ni–11.3Fe–1.4W Alloy

M. Spasojević[1], L. Ribić-Zelenović[1*)], N. Ćirović[2], P. Spasojević[3], A. Maričić[2]

[1]Faculty of Agronomy, University of Kragujevac, Čačak, Serbia
[2]Joint Laboratory for Advanced Materials of SASA,Technical Faculty Čačak, University of Kragujevac, Čačak, Serbia
[3]Faculty of Technology and Metallurgy, University of Belgrade, Belgrade, Serbia

Abstract:

A nanostructured Ni–11.3Fe–1.4W alloy deposit was obtained from an ammonium citrate bath at a current density of 600 mAcm^{-2}. XRD analysis shows that the deposit contains an amorphous matrix having embedded nanocrystals of the FCC phase of the solid solution of Fe and W in Ni with the average crystal grain size of 8.8 nm. The deposit has a high internal microstrain value and a high minimum density of chaotically distributed dislocations.

The effect of milling and annealing of the Ni–11.3Fe–1.4W alloy on electrical and magnetic properties was studied. Structural changes in the alloy take place during both annealing and milling. Upon deposition, the alloy was heated to 420^{0}C. Heating resulted in structural relaxation which induced a decrease in electrical resistivity and an increase in magnetic permeability of the alloy. Further heating of the alloy at temperatures higher than 420^{0}C led to crystallization which caused a reduction in both electrical resistivity and magnetic permeability.

The milling of the alloy for up to 12 hours caused a certain degree of structural relaxation and crystallization of the alloy. The increase in crystal grain size up to 11 nm and the partial structural relaxation induced a decrease in electrical resistivity and an increase in magnetic permeability of the alloy. Heating the powders obtained by milling at 420^{0}C led to complete structural relaxation, reduced electrical resistivity, and increased magnetic permeability. During heating of the powders obtained by milling at temperatures above 420^{0}C, crystallization and a significant increase in crystal grain size occurred, leading to a reduction in both electrical resistivity and magnetic permeability. The best magnetic properties were exhibited by the alloys milled for 12 hours and annealed thereafter at 420^{0}C. In these alloys, crystal grains were found to have an optimum size, and complete relaxation took place, resulting in a maximum increase in magnetic permeability.

Keywords: *Nickel-iron-tungsten alloys, Milling, Annealing, Magnetic properties*

1. Introduction

Nanostructured powders of different alloys are widely used in novel technologies due to their specific combinations of electrical, magnetic, catalytic, corrosion and other properties

*) **Corresponding author**: lenka@tfc.kg.ac.rs

[1-5]. Nanostructured nickel/iron/tungsten alloys are characterized by good electrical and magnetic properties, high corrosion and heat stability, and high catalytic activity for the cathodic evolution of hydrogen [6-17]. The metallurgic production of these alloys is expensive due to a high melting point of tungsten. Therefore, other procedures for their production have been developed, such as mechanical alloying, sputtering or electrolytic deposition from water baths [6-17]. The electrolytic procedure seems to be the most convenient method for the production of this alloy.

Electrodeposition can produce high purity alloy powders that have a specific microstructure and morphology whose properties considerably differ from those of the powders of identical chemical composition that are obtained by other methods [18-24]. The chemical composition, phase structure, shape and size of particles of the electrochemically obtained powders are dependent upon deposition current density, bath composition, temperature and circulation rate of the solution, and nature of the cathode material [18-24].

It is well-known that pure Mo and pure W cannot deposit electrochemically from molybdate/tungstate solutions [18]. However, if iron-group metal ions are present in the tungstate (molybdate) solution, different tungsten (molybdenum) alloys can be electrodeposited [25-33]. A huge scientific effort has been devoted to the explanation of the mechanism of deposition of W and Mo with iron-group metals, with the correlation between alloy composition and deposition conditions being observed [25-33].

M.L. Holt and L.E. Voaler [25] used the catalytic reduction theory to assume that the deposit consists of alternate thin layers of tungsten and iron-group metals.

A mechanism was proposed based on the hypothesis that iron-group metals and tungsten-containing ions form mixed electrochemically reducible complexes in the solution or on electrode surface [26, 27]. However, no presence of mixed complexes in the solution has been identified to date.

Chassaing et al. [28] observed that the multi-step reduction of molybdate (tungstate) leads to an intermediary Mo (IV)-oxide, which is further reduced by metal atoms of the iron-group metals.

Investigations into the deposition of Mo with metal atoms of the iron-group metals from citrate electrolytes led to a hypothesis based on the adsorption and catalytic reduction of molybdate species [29-31]. According to this mechanism, the species such as $[Me(II)HCit]^-$ catalyzes the reduction of molybdates forming an adsorbed reaction intermediate $[Me(II)HCit\text{-}MoO_2]_{ads}$ (where HCit denotes triply deprotonated citric acid, $C_6H_5O_7^{3-}$, and Me stands for iron-group metals).

This theoretical model is based on the fact that Mo deposition is possible only in the presence of Me(II) ions in the solution, with the reduction of Me ions following an independent path [29-31].

Obradović et al. [32] proposed a mechanism of tungsten and nickel codeposition from an ammonia-citrate electrolyte according to which two parallel reactions take place during alloy formation, i.e. nickel deposition from ammonia-citrate complexes and reduction of the protonated tungstate-citrate complex having more than one proton to lower valence oxides. The resulting nickel adatoms Ni(0) diffuse along the surface until they reach a crystal lattice point. Before they reach the crystal lattice point, part of these adatoms reach the low valence tungstate citrate complex and reduce it to metal tungsten. The chemical composition, microstructure and morphology of the deposit depend on the ratio of the parallel reduction reaction rates. The parallel hydrogen evolution reaction does not affect the chemical composition and microstructure; it affects the current efficiency of alloy deposition and, partly, the morphology [32].

Donten et al. [13] obtained smooth hard amorphous Fe-Ni-W alloy coatings from a citrate bath. The best properties were found in coatings with 50 at.% Fe. Pulse electroplating gave smoother and more uniform coatings with a higher content of W. The increase in W

content from 19 to 29 at.% led to improved hardness (Ni_{16} $Fe_{55}W_{29}$ alloys exhibit maximum 1070 HV).

He et al. [14] also deposited adherent smooth Ni-Fe-W alloy coatings with different W contents from a citrate bath on iron and steel substrates. As-plated deposits with 18 wt.% tungsten are crystalline FCC structure of nickel, while those with 35 wt.% and 55wt.% tungsten are amorphous. After heat treatments at about 700^0C deposits with 35 wt.% W obtain excellent corrosion resistance and have satisfactory wear resistance and microhardness.

Esther et al. [15] obtained smooth adherent crystalline coatings of Ni-Fe-W alloy from a citrate bath. The content of W of the coatings was found to increase, and that of Ni to decrease with increasing citrate concentration in the bath. All deposits contained nanocrystals of the FCC-structured solid solution of Fe and W in Ni. An increase in W content of the alloy induced a decrease in mean crystal size, and an increase in internal microstrains.

Deposits with 14 wt.%W exibit the best soft magnetic properties of the saturation magnetic flux density Bs = 0.99 T and coercivity Hc = 8 Oe. As the W content increases, the saturation magnetic flux density decreases whereas coercivity increases.

It should be noted that Ni-Fe-W alloys with high Ni concentration ($\geq$ 80 at.%) and Fe addition lower than 7 at.% exhibit a low Curie temperature ($Tc \leq 190K$) [16]. Sriraman et al. [11,12] showed that increasing current density of electrodeposition of Ni-Fe-W alloy from a citrate bath induced an increase in W and Fe content of the deposited alloy, and a decrease in both Ni content and crystal size of the FCC-structured solid solution of W and Fe in Ni. The corrosion resistance of the alloy increased with W content up to 9.2 at.% and then decreased [11,12].

Mun et al. [33] found that the content of Fe and W in smooth coatings of Ni-Fe-W alloys deposited from a citrate bath in the presence of 2-butane-1.4 diol and sodium lauzyl increases with increasing concentration of Fe^{2+} ions in the solution. The microhardness of the as-deposited specimen slightly increased with increasing W content in the deposit. Heat treatment remarkably improved the microhardness of the alloys, especially at 500^0C. However, the microhardness was markedly decreased with increasing grain size at temperatures over 500^0C.

Nanostructured alloys occur in a metasTab. state. Milling and heating change their microstructural properties. Annealing at relatively lower temperatures leads to structural relaxation in the alloys, and that at higher temperatures causes crystallization, resulting in a change in their mechanical, electrical, magnetic and other properties [34-36]. Structural relaxation induces the following changes: free volume decreases, resulting in decreased diffusion mass transfer, and partial arrangement of the alloy structure takes place, increasing its readiness to crystallize [37,38]. During crystallization, an arranged structure is formed and significant changes in the physico-chemical properties of the alloy occur.

The objective of this study was to obtain a Ni-Fe-W alloy having adequate magnetic characteristics and evaluate the effect of milling and annealing at different temperatures on the microstructure and electrical and magnetic properties of the alloy.

2. Experimental

The nickel/iron/tungsten alloy composed of 87.3 wt.% Ni, 11.3 wt.% Fe and 1.4 wt.% W (Ni–11.3Fe–1.4W) was obtained by electrodeposition from an ammonium citrate bath. The glass electrochemical cell was 8 dm^3. The anode was a 12 cm^2 platinum plate placed at a spacing of 1.0 cm in parallel with the titanium plate-shaped cathode 4 cm^2 in area and 0.2 cm in thickness. The cell was in a thermostat at a temperature of 60 ± 0.5^0C. The solution was prepared from p.a. chemicals and triple distilled water. The solution composition was: 0.2 $moldm^{-3}$ $NiSO_4 \cdot 7H_2O$, 0.02 $moldm^{-3}$ $FeSO_4$, 0.004 $moldm^{-3}$ $Na_2WO_4 \cdot 2H_2O$, 0.23 $moldm^{-3}$ $Na_3C_6H_5O_7 \cdot 2H_2O$, 3.2 $moldm^{-3}$ NH_4Cl, 0.3 $moldm^{-3}$ Na_2SO_4. The pH of the solution was

adjusted by addition of 0.7 mol/dm^{-3} NH_4OH, and it ranged from 9.3 to 9.4. During the electrolysis, a standard electrical circuit was used. The alloy was deposited galvanostatically at a current density of 600 mAcm^{-2}. Upon electrolysis, the deposit was washed several times with distilled water and, then, with 0.1% wt.% benzoic acid solution in order to prevent oxidation. Thereafter, the deposit was dried at 105^{0}C.

Scanning electron microscopy (SEM) analysis was performed by a JEOL – JSM 5300 equipped with on a EDS – QX2000 spectrometer. The chemical composition of the alloy was determined by energy dispersive X-ray spectroscopy (EDS) using attachment to SEM as well as by atomic absorption (PEKTAR-AA200-VARIAN).

X-ray diffraction (XRD) was recorded on a Philips PW 1710 diffractometer using $Cu_{k\alpha}$ radiation (λ = 0.154 nm) and a graphite monochromator. XRD data were collected with a step mode of 0.03^0 and collection time of 1.5 s/step.

The as-prepared alloy was milled in an alcohol medium using a Planetary Ball Mill Type PM 400.

The electrical properties were investigated using 40x1.2x0.5 mm^3 samples, obtained by exposing the deposit to the pressure of 100 MPa. Electrical resistivity was measured by the four-point method within the temperature interval of 20-640^{0}C. The measurements were made in an argon atmosphere. The measurements of relative magnetic permeability were performed using a modified Maxwell method, based on the action of an inhomogeneous field on the magnetic sample. The magnetic force measurements were performed with a sensitivity of 10^{-6} N in an argon atmosphere.

3. Results and discussion

The highly porous spongy deposit of Ni–11.3Fe–1.4W alloy was obtained by electrodeposition from an ammonium citrate bath at a current density of 600 mAcm^{-2}. The chemical composition of the nickel/iron/tungsten alloy was determined by both atomic absorption and EDS analysis. The results obtained showed differences of less than 1 wt.%. The powder contained 87.3 wt.% Ni, 11.3 wt.% Fe and 1.4 wt.% W (Ni–11.3Fe–1.4W).

The phase structure of the deposit was determined by XRD analysis. Fig. 1. shows a Reitveld's diagram for the as-prepared Ni–11.3Fe–1.4W alloy.

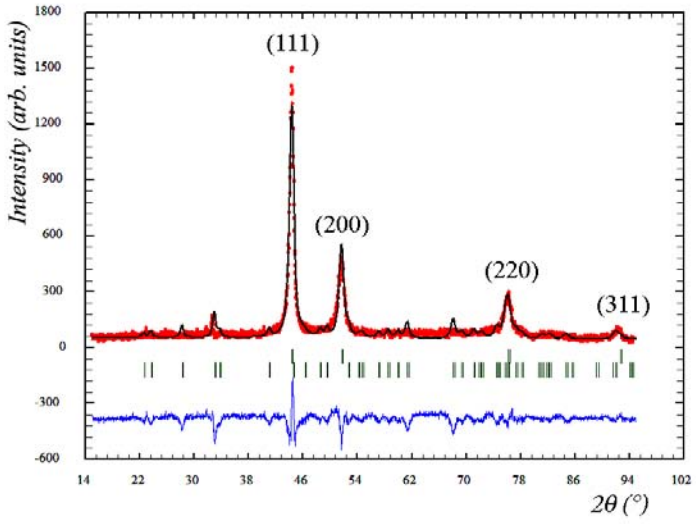

Fig. 1. Reitveld's diagram for the as-prepared Ni–11.3Fe–1.4W alloy.

The observed data points are presented by dots; the upper solid line represents values calculated for the given structural model, and the difference between the observed and calculated data points is plotted at the bottom. Vertical lines represent positions of Bragg reflections: the first line corresponds to the positions of the peaks for the FC phase of the solid solution of W and Fe in Ni, the second line to positions of the peaks for the WO_3 structure in the P4/nmm space group structure.

The diagram exhibits well pronounced peaks only for the FCC phase of the solid solution of W and Fe in Ni. The extremely weak peaks of the WO_3 structure indicate the negligible presence of the crystal phase in the test sample.

The diagram shows no peaks for the BCC phase of iron or tungsten, or peaks for the intermetal compounds of the three metals. The presence of the FCC phase in alloys containing less than 18 wt.% of tungsten was observed in studies [11,12,14,15,17,33 and 39]. The peaks are relatively wide, low in intensity and shift towards lower 2θ values as compared to the values for the pure nickel FCC phase. This is the result of the presence of small crystal grains of the Ni–11.3Fe–1.4W alloy. The high electrodeposition current density and the presence of tungsten in the solid solution caused the formation of both the amorphous phase and nanocrystals that have small crystal grains, a high mean microstrain value and a high minimum density of chaotically distributed dislocations (Tab. I) [5,22,39,40].

Tab. I. Microstructural data of the crystalline phase (FCC) of the Ni–11.3Fe–1.4W alloy powder

Current density (mA cm^{-2})	Unit cell parameters (nm)	Mean crystallite size value (nm)	Mean microstrain value	Minimum density of chaotically distributed dislocations (cm^{-2})
600	a=0.35324(5)	8.8	$2.3 \cdot 10^{-3}$	$3.9 \cdot 10^{12}$

The highest peak intensity (111) indicates texture existence. The development of this texture was associated with the preferred growth along (111) orientation due to lower strain associated in that direction [117,41].

The relatively low intensity of FCC phase peaks and the relatively low mean crystallite size value (8.8 nm) show that the as-prepared Ni–11.3Fe–1.4W alloy contains not only the FCC phase of the solid solution of tungsten and iron in nickel, but also the amorphous phase. The presence of the two phases in the electrochemically obtained nickel/iron/tungsten alloys was also reported in other works [14,17,33,39].

Transmission electron microscopic observations of the electrodeposited Ni-W binary alloy also showed nanocrystals to be distributed in an amorphous matrix [11].

The X-ray diagram of the alloy annealed for 60 minutes at 420^0C is identical to that for the as-prepared alloy, suggesting that annealing the Ni–11.3Fe–1.4W alloy at temperatures below 420^0C does not result in the crystallization of the amorphous phase and crystal grain growth of the FCC phase.

However, the X-ray diagram of the alloy annealed for 60 minutes at 650^0C has narrow peaks and high intensity peaks (Fig. 2). This suggests that annealing at 650^0C led to the crystallization of the amorphous phase and crystal grain growth of the FCC phase accompanied with a simultaneous decline in both microstrain and minimum density of chaotically distributed dislocations (Tab. II).

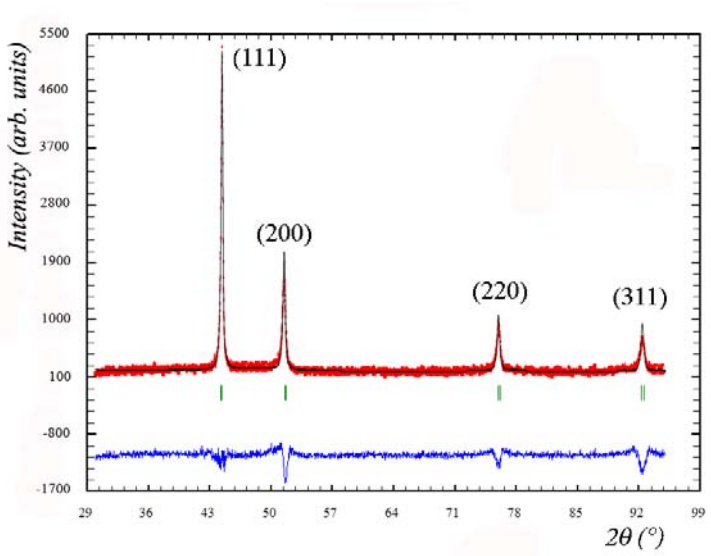

Fig. 2. Reitveld's diagram for the alloy annealed for 60 minutes at 600^0C.

The observed data points are presented by dots; the upper solid line represents values calculated for the given structural model, and the difference between the observed and calculated data points is plotted at the bottom. Vertical lines represent positions of Bragg reflections for the FCC phase.

Tab. II. Microstructural data of the crystalline phase (FCC) of the Ni–11.3Fe–1.4W alloy annealed for 60 minutes at 650^0C

Current density (mA cm^{-2})	Unit cell parameters (nm)	Mean crystallite size value (nm)	Mean microstrain value	Minimum density of chaotically distributed dislocations (cm^{-2})
600	a=0.36050(4)	22.5	$0.4 \cdot 10^{-3}$	$0.1 \cdot 10^{12}$

The samples of the electrochemically produced alloys were milled for 4, 8 and 12 hours, and their X-rays were recorded. The increase in milling time induced an increase in the intensity of FCC phase peaks, and a decrease in their half-height width (Fig. 3). This indicates that milling gives rise to partial crystallization of the amorphous phase, and causes FCC-phase crystal grain growth with a simultaneous decrease in microstrain and minimum density of chaotically distributed dislocations (Tab. III).

Tab. III. Microstructural data of the crystalline phase (FCC) of the Ni–11.3Fe–1.4W alloy milled for 12 hours

Current density (mA cm^{-2})	Unit cell parameters (nm)	Mean crystallite size value (nm)	Mean microstrain value	Minimum density of chaotically distributed dislocations (cm^{-2})
600	*a*=0.35430(2)	11.1	$1.8 \cdot 10^{-3}$	$2.4 \cdot 10^{12}$

The as-prepared deposit of the Ni–11.3Fe–1.4W alloy composed of an amorphous matrix and nanocrystals (8.8 nm) of the FCC phase having a high internal microstrain value and a high minimum density of chaotically distributed dislocations is relatively thermally unsTab.. Heating during the milling process causes partial crystallization of the amorphous

phase and an increase in FCC-phase crystal grain size, along with a reduction in both internal microstrain value and minimum density of chaotically distributed dislocations. These microstructural changes induce changes in the magnetic and electrical properties of the deposit.

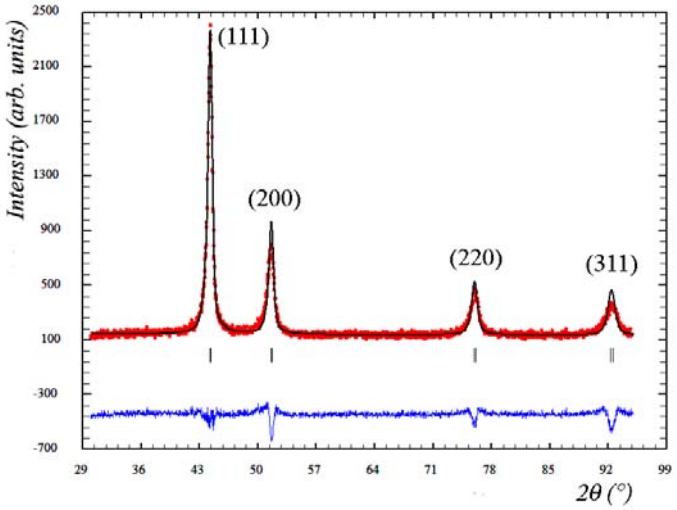

Fig. 3. Reitveld's diagram for the Ni–11.3Fe–1.4W alloy milled for 12 hours.

The observed data points are presented by dots; the upper solid line represents values calculated for the given structural model, and the difference between the observed and calculated data points is plotted at the bottom. Vertical lines represent positions of Bragg reflections for the FCC phase.

The structural changes in the electrochemically obtained Ni–11.3Fe–1.4W alloy during heating were monitored by measurements of changes in electrical resistivity. Fig. 4. presents the temperature dependence of the electrical resistivity of the as-prepared deposit and milled powders.

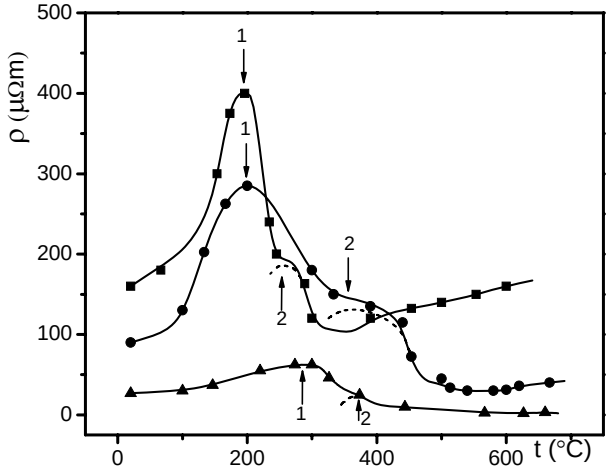

Fig. 4. Temperature dependence of electrical resistivity: ■– as-prepared deposit; ●- powder milled for 8 hours, and ▲- powder milled for 12 hours. Heating rate 20^0C min^{-1}.

As shown in Fig. 4, resistivity was highest for the as-prepared deposit, and lowest for the powder milled for 12 hours. The increase in milling time results in a decrease in resistivity. All diagrams show the appearance of a single maximum (1) and a single shoulder (2).

The decrease in resistivity after the maximum was due to structural changes taking place during relaxation processes most likely in the amorphous phase. The decrease in resistivity after the shoulder was the result of structural changes taking place during relaxation processes occurring most likely in nanocrystals. Heating the powder during structural relaxation induces short-term structural arrangement. Then, certain high-energy atoms cross the energy barrier and reach the somewhat lower potential level. At this lower level, their 3d and 4s orbitals overlap better with identical orbitals of neighboring atoms, thereby contributing to an increase in electron density in the conduction zone near the Fermi level. Structural arrangement in both the amorphous phase and nanocrystals results in increased mean length of the free electron path. The increase in electron density at the Fermi level and the increase in the mean length of the free electron path induce a reduction in electrical resistivity [622]. Resistivity decreases with increasing milling time: a) due to the fact that milling gives smaller particles which establish better mutual contact during pressing, and b) due to the fact that during milling, part of the amorphous phase, as induced by the energy input, is transformed into a crystal FCC phase, with existing crystal grains of the FCC phase growing simultaneously with a decrease in both mean microstrain value and minimum density of chaotically distributed dislocations (Tab.s 1 and 3). The process under b) causes a reduction in peak intensity and shoulder intensity, as well as a shift in peak maximum and shoulder temperatures towards higher temperatures.

Furthermore, the microstructural changes of the alloy during heating cause changes in relative magnetic permeability. Fig. 2. shows changes in relative magnetic permeability of the as-prepared alloy during heating. The curve represented by a solid triangle (▲) shows an increase in relative magnetic permeability of the as-prepared alloy during the first heating within the temperature range of 80^0C to 380^0C. Further heating in the temperature range of 380^0C to 500^0C induces no changes in magnetic permeability. After the first heating up to 500^0C, the alloy was cooled to room temperature. During cooling, no changes were observed in relative magnetic permeability. This suggests that irreversible structural changes occurred in the alloy during the structural relaxation taking place in the heating process. Following these irreversible structural changes, the sample cooled to room temperature had about 8% higher magnetic permeability than the as-prepared alloy. This increase was induced by structural relaxation during the first heating. During structural relaxation, short-range structural arrangement took place in the alloy, as induced by the effect of heat and external 8000 Am^{-1} magnetic field. The short-range structural arrangement causes atoms to translocate into a somewhat lower energy level. At the lower energy level, the atoms existing between the magnetic domain walls attach to the energetically more favorable domain. The simultaneous decrease in the density of chaotically distributed dislocations causes higher mobility of magnetic domain walls, facilitating their orientation in the external magnetic field. This leads to magnetic domain expansion and, hence, increased magnetization and increased magnetic permeability.

After the first heating, the cooled sample was reheated up to 600^0C. During the second heating, magnetic permeability did not undergo substantial changes up to 500^0C. This suggests that no significant structural changes occurred in the alloy during the second heating up to 500^0C.

During the second heating in the temperature range of 500^0C to 600^0C, the increase in temperature results in an abrupt decline in relative magnetic permeability. The decline is caused by the change in the orientation of certain domains due to the effect of thermal energy and structural changes in the alloy. At temperatures above 450^0C, the crystallization of the amorphous phase and crystal grain growth of the FCC phase take place. The crystallized alloy

having larger crystal grains has lower magnetic permeability as compared to the as-prepared alloy. In the alloy with larger crystal grains, orientation of certain domains is hampered, and the walls of oriented domains show lower mobility.

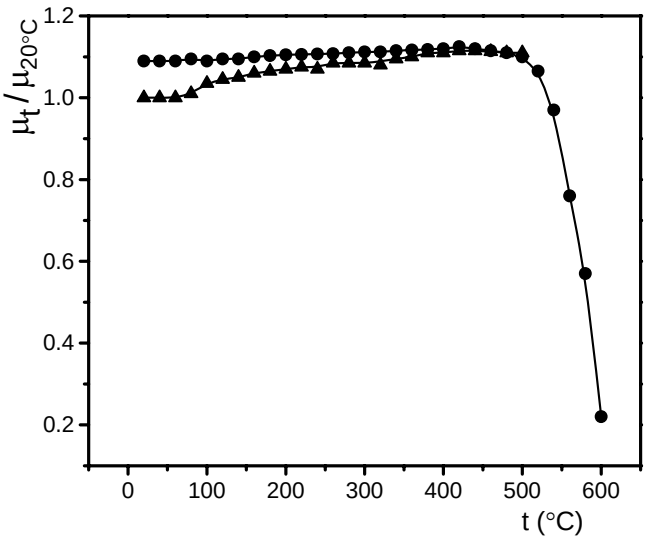

Fig. 5. Temperature dependence of the relative magnetic permeability of Ni–11.3Fe–1.4W alloy: ▲– first heating up to 500^0C and ●– second heating up to 600^0C. The heating rate was 20^0C min^{-1}.

Fig. 6. presents the temperature dependence of the relative magnetic permeability of the Ni–11.3Fe–1.4W alloy powder obtained after eight hours of milling.

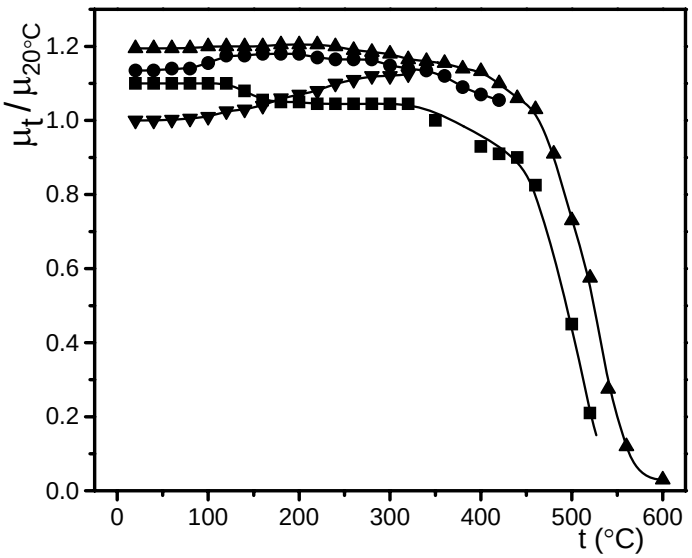

Fig.6. Temperature dependence of the relative magnetic permeability of the Ni–11.3Fe–1.4W powder obtained after eight hours of milling: ▼- first heating up to 350^0C, ● – second heating up to 420^0C, ▲– third heating up to 600^0C, ■- fourth heating up to 520^0C. The heating rate was 20^0C min^{-1}.

Fig. 6. shows that heating the milled powder for eight hours up to 350^0C causes partial structural relaxation in the powder. Complete structural relaxation does not occur until after

the second heating up to 420^{0}C. Therefore, its relative magnetic permeability does not change during the third heating from root temperature to 300^0. Further heating from 300^{0}C to 450^{0}C results in a gradual decline in relative magnetic permeability. The abrupt decline in permeability takes place within the temperature range of 450^{0}C to 560^{0}C. Following the third heating up to 600^{0}C, the powder was cooled, and reheated again for the fourth time. During the fourth heating, the relative magnetic permeability was lower than during the third heating. This decrease was induced by powder crystallization during the third heating within the temperature range of 450^{0}C to 600^{0}C.

Fig. 7. presents the temperature dependence of the relative magnetic permeability of the Ni–11.3Fe–1.4W alloy powder obtained after 12 hours of milling.

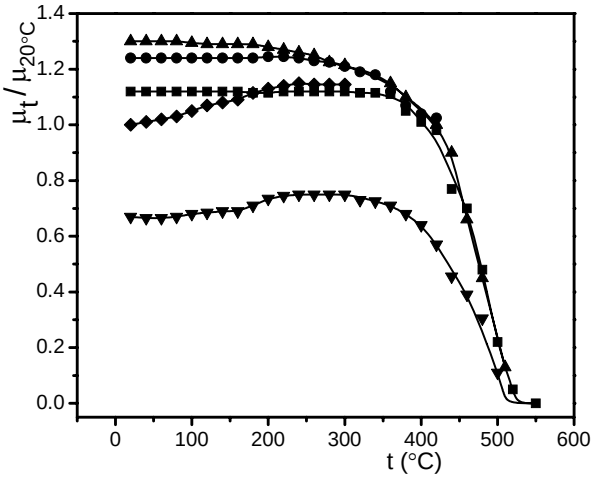

Fig. 7. Temperature dependence of the relative magnetic permeability of the Ni–11.3Fe–1.4W powder obtained after 12 hours of milling: ◆- first heating up to 300^{0}C, ● – second heating up to 420^{0}C; ▲– third heating up to 510^{0}C, ■ - fourth heating 600^{0}C, ▼- fifth heating up to 600^{0}C. The heating rate 20^{0}C min^{-1}.

Fig. 7. shows that complete structural relaxation takes place during powder heating up to 420^{0}C. The complete relaxation induces a maximum increase in relative magnetic permeability. Heating the powder up to 510^{0}C causes a decline in relative magnetic permeability. The decline is considerably higher during heating up to 600^{0}C. At higher temperatures, the crystallization process is more complete, resulting in a higher reduction in relative magnetic permeability.

The diagrams presented in Fig. 8 show that magnetization of both non-annealed and annealed powders increases with increasing milling time.

The analysis of the above diagrams suggests the following:

a) as a result of the annealing of the as-prepared deposit and the powders produced by milling at 420^{0}C, complete structural relaxation takes place in the alloy, causing a maximum increase in relative magnetic permeability for the given crystal grain size.

b) at temperatures above 420^{0}C, the amorphous part of the alloy undergoes crystallization, and crystal grain growth of the solid solution of iron and tungsten in nickel occurs, inducing a decline in magnetic permeability.

c) the increase in milling time results in: 1. – increasing magnetization of the powders, 2. – a reduction in relative magnetic permeability at lower temperatures, and 3.- a shift of the Curie point to lower temperatures.

d) the annealing of the powders at the temperature range of 450^{0}C to 600^{0}C causes a decrease in their Curie temperatures.

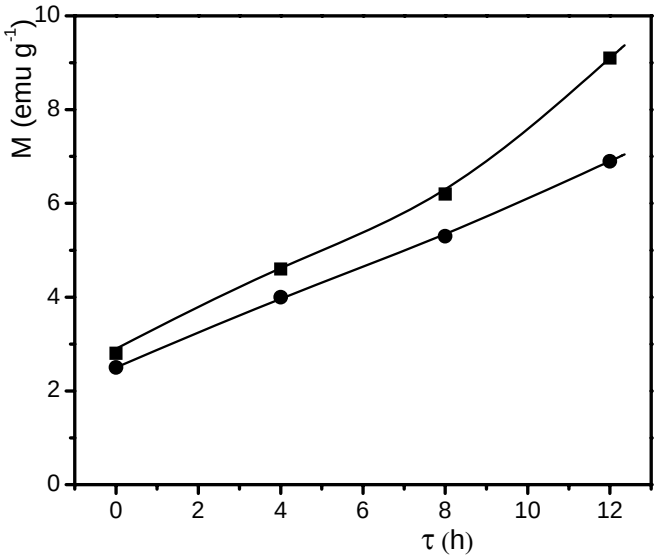

Fig. 8. shows magnetization as a function of milling time: ●– non-annealed powders, ■- powders heated up to 420^0C.

Structural changes in the Ni–11.3Fe–1.4W alloy take place both during annealing and milling, involving structural relaxation which induces a decrease in electrical resistivity and an increase in magnetic permeability.

Both processes: annealing at temperatures above 450^0C and milling at room temperature cause crystallization of the amorphous phase in the alloy, crystal grain growth of the FCC phase, and a simultaneous reduction in both the mean microstrain value and minimum density of chaotically distributed dislocations. During the milling of the as-obtained alloy for 0.0 to 12 hours, the mean value of crystal grains increases from 8.8 nm to 11.1 nm. During the 60-minute annealing of the as-obtained alloy at 600^0C, crystal grain size increases from 8.8 nm to 22.5 nm, and that of the powder milled for 12 hours from 11.1 nm to 25.9 nm. The experimental data show that the electrical and magnetic properties of the Ni–11.3Fe–1.4W alloy are dependent upon crystal grain size. The magnetic permeability initially increases with increasing crystal grain size, reaching its maximum and decreasing thereafter with further increase in the mean value of crystal grain size. Electrical resistivity starts to decrease abruptly and then declines gradually with increasing crystal grain size. The experimental results suggest that the use of annealing and milling parameters results in the production of Ni–11.3Fe–1.4W alloy powders that have specific magnetic and electrical properties.

4. Conclusions

A nanostructured Ni–11.3Fe–1.4W alloy was obtained by electrodeposition from an ammonium citrate electrolyte at a current density of 600 mA cm^{-2}.

XRD analysis showed that the alloy contains an amorphous matrix having embedded nanocrystals of the FCC solid solution of iron and tungsten in nickel, with an average crystal grain size of 8.8 nm, a high internal microstrain value and a high density of chaotically distributed dislocations. Structural changes in the Ni–11.3Fe–1.4W alloy take place both during annealing and milling. As a result of heating at 420^0C, structural relaxation occurs,

inducing a decrease in electrical resistivity and an increase in magnetic permeability of the alloy. During the annealing of the alloy at temperatures above 420^0C, crystallization takes place, leading to a reduction in both electrical resistivity and magnetic permeability.

The milling of the alloy for up to 12 hours caused a certain degree of structural relaxation and crystallization in the alloy. The increase in crystal grain size up to 11 nm and the partial structural relaxation induce a decrease in electrical resistivity and an increase in magnetic permeability of the alloy. Heating the powders obtained by milling up to 420^0C leads to complete structural relaxation, reduced electrical resistivity, and increased magnetic permeability. During heating of the powders obtained by milling at temperatures above 420^0C, crystallization and a significant increase in crystal grain size occur, leading to a reduction in both electrical resistivity and magnetic permeability. The best magnetic properties are exhibited by the alloys milled for 12 hours and annealed thereafter at 420^0C. In these alloys, crystal grains have an optimum size, and complete relaxation took place.

Acknowledgments

The authors acknowledge financial support from the Ministry of Education and Science of the Republic of Serbia through Project No. 172057.

References

1. P. Haasen, R.I. Joffe, Amorphous Metals and Semiconductors, Pergamon, London, 1986.
2. N.F. Motte, E.A. Davis, Electronic Processes in Non-Crystalline Materials, Claredon Press, Oxford, 1979.
3. H. Steerb, H. Warlimont, Rapidly Quenched Metals, Elsevier, Amsterdam, 1985.
4. A. Maričić, M. Spasojević, L. Rafailović, V. Milovanović, L. Ribić-Zelenović, Mater.Sci. Forum 453 (2004) 411-415.
5. L. Ribić-Zelenović, L. Rafailović, M. Spasojević, A. Maričić, Phys.B 403 (2008) 2148-2154.
6. S.H. Hong, H.J. Rya, Mater.Sci.Eng.A. 344 (2003) 253-260.
7. J.L. Fan, B.Y. Huang, X.I. Qu, Trans Nonferrous Met.Soc.China 10(1) (2000) 57-59.
8. Z.He, T.H. Courtney, Mater.Sci.Eng. A. 346 (2003) 141-148.
9. Z.W. Zhang, J.I.E.Zhou, S.Q.Xi, et al., J.Alloys Compd. 370 (2004) 186-191.
10. Z.W.Zhang, J.N.Zhou, S.Q.Xi, Mater.Sci.Eng A 379 (2004) 148-153.
11. K.R. Sriraman, S. G. Raman, S.K. Seshadri, Mater.Sci,Eng. A 418 (2006) 303-311.
12. K.R. Sriraman, S.Ganesh Sundara Raman, S.K. Seshadri, Mater.Sci.Technol. 22 (2006) 14-20.
13. M. Donten, H. Cesiulis, Z. Stojek, Electrochim. Acta 39 (2000) 3389-3396.
14. F. He, J. Yang, T. Lei, C. Gu, Appl. Surf. Sci. 253 (2007) 7591-7598.
15. P. Esther, C. Joseph Kennady, P. Saravanan, T. Venkatachalam, J. Non-Oxide Glasses, 1(2009) 301-309.
16. M. Banerjee, A. Singh, A.K. Majumdar, A. K. Nigam, J. Phys.: Condens. Matter 23 (2011) 3060004.
17. L. Ribić-Zelenović, N. Ćirović, M. Spasojević, N. Mitrović, A. Maričić, V. Pavlović, Mater. Chem. Phys. (2012), doi: 10.1016/j.matchemphys.2012.04.061
18. A. R. Despić, K. I. Popov, Modern Aspects of Electrochemistry, vol. 7, Plenum Press, New York, 1972.
19. M. Spasojević, L. Ribić-Zelenović, A. Maričić, Sci. Sinter. 43 (2011) 313-327.
20. M. G. Pavlović, Lj. J. Pavlović, E. R. Ivanović, V. Radmilović, K. I. Popov, J. Serb. Chem. Soc.66 (2001) 923-933.

21. L. Ribić-Zelenović, M. Spasojević, A. Maričić, M. M. Ristić, Sci. Sinter. 41 (2) (2009) 175-184.
22. L. Ribić-Zelenović, M. Spasojević, A. Maričić, Materials Chemistry and Physics, 115 (2009) 347-351.
23. M. A. Meyers, A. Mishra, D. J. Benson, Progress in Materials Science, 51 (2006) 427-556.
24. K. I. Popov, M. G. Pavlović, in. B. E. Conway, J. O'M. Bockris, R. E. White (Eds.), Electrodeposition of Metal Powders with Controlled Particles Grains Size and Morphology in Modern Aspects of Electrochemistry, Vol. 24, Plenum, New York, 1973, pp. 299-391.
25. M. L. Holt, L. E. Vaaler, J. Electrochem. Soc. 94 (1948) 50-58.
26. O. Younes, E. Gileadi, Electrochem. Solid State Lett. 3 (2000) 543-545.
27. O. Younes, L. Zhu, Y. Rosenberg, Y. Shacham-Diamond, E. Gileadi, Langmuir 17 (2001) 8270-8275.
28. E. Chassaing, K.Vu Quang, R. Wiart, J. Appl. Electrochem. 19 (1989) 839-844.
29. D. Landolt, E.J. Podlaha, N. Zech, Zh. Phys. Chem. 208 (1999) 167-182.
30. E. J. Podlaha, D. Landolt, J. Electrochem. Soc. 143 (1996) 893-899.
31. E. J. Podlaha, D. Landolt, J. Electrochem. Soc. 144 (1997) 1672-1680.
32. M. D. Obradović, R. M. Stevanović, A. R. Despić, J. Electroanal. Chem. 552 (2003) 185-196.
33. Seong-Joe Mun, Minsoo, Toe-Hong Yim, Joe-ho Lee, Tak Kang, J. Electrochem.Soc. 157 (2010) D177-D180.
34. 13. G. Herzer, IEEE Trans. Magn. 25 (1989) 3327-3329.
35. S. Roth, H. Grahl, J. Degmova, N. Schlorke-de Boer, M. Stoica, J.M. Borrego, A. Conde, N. Mitrović, J. Eckert, J. Optoelectron. Adv. Mater. 4 (2002) 199-205.
36. N. Mitrović, J. Magn. Magn. Mater. 262 (2003) 302-307.
37. J. D. Bernal, Nature 185 (1960) 68-70.
38. A. Kalezić-Glišović, V. A. Maričić, D. A. Kosanović, S. Đukić, R. Simeunović, Sci. Sinter. 41 (2009) 283-291.
39. K.R. Sriraman, S. Ganesh Sundara Raman, S.K. Seshadri, Mater. Sci. Eng.A 460-461 (2007) 39-45.
40. L.Ribić-Zelenović, R.Simeunović, A.Maričić, M.Spasojević, Mater. Sci.Forum. 555 (2007) 539-543.
41. H.Wang, S.Yao, S.Matsumura, Surf.Coat. Technol. 157 (2002) 166-170.

Садржај: *Наноструктурни депозит легуре Ni–11,3Fe–1,4W добијен је електродепозицијом из амонијачно-цитратног купатила на густини струје 600 mAcm^{-2}. XRD анализа је показала да се депозит састоји од аморфне матрице у којој су смештени нанокристали FCC фазе чврстог раствора Fe и W у Ni чије су просечне димензије 8,8 nm. Проучаван је утицај млевења и одгревања легуре Ni–11,3Fe–1,4W на електрична и магнетна својства. Структурне промене легуре се одигравају и током одгревања и током млевења. Одмах након депоновања легура је загревана до 420^{0}C. Током загревања дошло је до процеса структурне релаксације која је узроковала смањење електричне отпорности и повећање магнетне пермеабилности легуре. Даљим загревањем легуре на температурама вишим од 420^{0}C одвија се процес кристализације који доводи до смањења и електричне отпорности и магнетне пермеабилности.*

Млевењем легуре до 12 часова у легури се у извесној мери одвијају и процес структурне релаксације и процес кристализације. Пораст кристалних зрна до 11 nm и делимична структурна релаксација узрокују смањење електричне отпорности и

повећање магнетне пермеабилности легуре. Загревањем прахова добијених млевењем до 420^{0}C долази до потпуне структурне релаксације, смањења електричне отпорности и повећање магнетне пермеабилности. Током загревања прахова добијених млевењем на температурама вишим од 420^{0}C долази до кристализације и значајног пораста величине кристалних зрна, а то доводи до смањења и електричне отпорности и магнетне пермеабилности. Најбоља магнетна својства имају легуре млевене 12 часова, а затим одгрејане на 420^{0}C. У овим легурама кристална зрна имају оптималну величину, а процес релаксације се потпуно одиграо, што узрокује максималан пораст магнетне пермеабилности.

Кључне речи: *никал-гвожђе-волфрам легуре, млевење, одгревање, магнетна својства*